

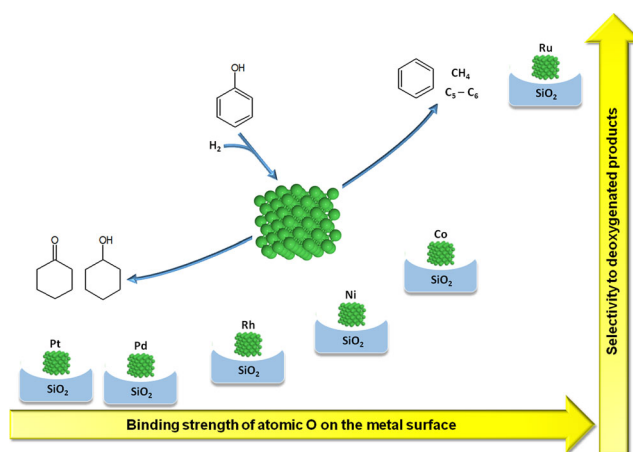
The Effect of Metal Type on Hydrodeoxygenation of Phenol Over Silica Supported Catalysts

Camila A. Teles^{1,2} · Raimundo C. Rabelo-Neto¹ · Jerusa R. de Lima³ · Lisiane V. Mattos³ · Daniel E. Resasco⁴ · Fabio B. Noronha^{1,2}

Received: 5 May 2016 / Accepted: 14 July 2016
© Springer Science+Business Media New York 2016

Abstract Different metals supported on SiO₂ were tested for the hydrodeoxygenation of phenol. For Pt/SiO₂, Pd/SiO₂ and Rh/SiO₂ catalysts, phenol is mainly tautomerized, followed by hydrogenation of the aromatic ring. The direct dehydroxylation of phenol followed by hydrogenolysis is favored over more oxophilic metals (Ru, Co and Ni).

Graphical Abstract



Keywords Phenol · SiO₂ · Hydrodeoxygenation · Tautomerization · Dehydroxylation · Biomass · Bio-oil

Electronic supplementary material The online version of this article (doi:10.1007/s10562-016-1815-5) contains supplementary material, which is available to authorized users.

✉ Fabio B. Noronha
fabio.bellot@int.gov.br

- ¹ Catalysis Division, National Institute of Technology, Rio de Janeiro 20081-312, Brazil
- ² Chemical Engineering Department, Military Institute of Engineering, Praça Gal. Tiburcio 80, Rio de Janeiro 22290-270, Brazil
- ³ Chemical Engineering Department, Fluminense Federal University, Rua Passo da Pátria 156, Niterói 24210-240, Brazil
- ⁴ School of Chemical, Biological, and Materials Engineering, Center for Biomass Refining, The University of Oklahoma, Norman, OK 73019, USA

1 Introduction

The bio-oil obtained from fast pyrolysis of lignocellulosic biomass has great potential for the production of liquid biofuels. However, the bio-oil contains a high amount of oxygen-containing compounds such as phenol, cresol, guaiacol, which are products from the decomposition of lignin fraction of the lignocellulosic biomass. Due to the high oxygen content, bio-oil exhibits a lower energy density compared to crude oil, high corrosivity and poor thermal stability [1, 2]. Therefore, bio-oil has to be upgraded to remove oxygen in order to be used as a fuel in vehicles, which may be achieved by hydrodeoxygenation (HDO) process [3]. Because of the complex composition of

bio-oil, several studies investigate the HDO reaction of model molecules representatives of specific fractions of the lignocellulosic biomass such as guaiacol, phenol, cresol.

The reaction mechanism for HDO of phenolic compounds such as phenol or cresol has been extensively studied in the literature in order to design more efficient catalysts for this process [4–16]. Three reaction pathways have been proposed in the literature [17]. The first one is based on the sequential hydrogenation (HYD) of the aromatic ring on metal sites followed by dehydration of cyclohexanol on acid sites. Therefore, this reaction pathway may take place on catalysts containing a support with sufficient acidity to catalyze the dehydration of the alcohol (cyclohexanol or 3-methylcyclohexanol) [18]. However, dehydration does not occur to a significant extent over silica or zirconia supported catalysts since these supports do not have significant acidity [12]. The second one is the so called direct deoxygenation (DDO) and involves the cleavage of the C–O bond in the phenolic molecule. This pathway requires a relatively high activation energy and therefore, it may occur depending on reaction temperature and catalyst used [19]. The third mechanism is the tautomerization of phenolic compound to a cyclohexadienone intermediate (2,4-cyclohexadienone or 3,5-methylcyclohexadienone) [10–12, 20, 21]. This intermediate may react by two different routes. For example, in the HDO of phenol, the hydrogenation of the ring, producing 2-cyclohexen-1-one that is hydrogenated to cyclohexanone and then cyclohexanol; or the hydrogenation of the carbonyl group, leading to the formation of 2,4-cyclohexadienol, which can in turn, convert to benzene. The differences in the reaction pathway strongly depend on the type of metal and support.

Nie et al. [10] studied the HDO of *m*-cresol in gas phase on SiO₂-supported Ni, Fe, and bimetallic Ni–Fe catalysts at 573 K and atmospheric pressure. Over the monometallic Ni catalyst, the dominant product was 3-methylcyclohexanone whereas toluene was the main product on Fe and Ni–Fe bimetallic catalysts. The differences in product distributions observed for Ni and Fe-containing catalysts were explained in terms of a reaction pathway based in a tautomerization step. According to this mechanism, *m*-cresol is tautomerized to a highly unstable methylcyclohexadienone intermediate that may react through two different routes. In the case of Group VIII metal catalysts such as Ni, Pt, or Pd that have a strong affinity for the aromatic ring, the cresol molecule adsorbs in parallel to the surface and they are highly active for ring hydrogenation. For oxophilic metals such as Fe and its alloys, the strong interaction of the oxygen from the carbonyl group of the keto tautomer intermediate and the oxophilic metal (in this work represented by unreduced metal) promotes its hydrogenation. In

this case, the cresol molecule adsorbs perpendicular to the surface, inhibiting the hydrogenation of the ring.

Experimental and theoretical calculations were used to investigate the mechanism of *m*-cresol over Pt/SiO₂ and Ru/SiO₂ catalysts in gas phase, at 573 K and atmospheric pressure [21]. 3-methylcyclohexanone was the main product formed over Pt/SiO₂ catalyst whereas toluene and C₁–C₅ hydrocarbons were mainly produced over Ru/SiO₂ catalyst. Density functional theory (DFT) methods were used to investigate the *m*-cresol conversion over the Pt (111) and Ru (0001) surfaces. The DFT results showed that the reaction proceeds through the tautomerization route over Pt (111) surface. However, the direct deoxygenation of *m*-cresol is preferred instead of the tautomerization route over Ru (0001) surface. This result was attributed to the stronger oxophilicity of Ru, which leads to a high energy barrier for the tautomerization pathway. In this case, an unsaturated hydrocarbon species is formed during the direct dehydroxylation of *m*-cresol, which undergoes hydrogenolysis to C₁–C₅ hydrocarbons. Hensley et al. [17] also suggested that the direct deoxygenation occurs on the HDO of phenol over Fe (110) surface. However, the activation energy barrier and reaction energies for the C–O bond cleavage are larger on Pd (111) and thus, this surface is not active for deoxygenation. In both studies, the direct deoxygenation occurred on the more oxophilic metal.

Different catalysts have been studied for HDO of phenolic compounds such as phenol or cresol, including supported noble metals (Pd, Pt, Rh, Ru) [1, 6, 10, 11, 16, 22–29] supported base metals (Ni, Co, Fe, Cu) [6, 30–33] and bimetallic catalysts [10, 26]. However, studies comparing the performance of a series of catalysts with different metals are scarce and only few were carried out in gas phase but in these cases, the HDO of *m*-cresol was investigated [10, 29].

Therefore, there has been no systematic study for the HDO of phenol reaction over a wide range of metals under the same conditions, investigating the effect of the type of the metal on reaction pathways. However, the mechanism of HDO of phenol consists of a metallic particle and a Lewis acid site of the support and the reaction takes place in the metal-support interface. Then, in order to obtain a better understanding of the effect of the type of the metal on the HDO of phenol, it is fundamental the use of an inert support such as silica that does not exhibit Lewis acid sites.

The goal of this work is to investigate the effect of the metal type on the HDO of phenol over silica supported catalysts. A systematic study was performed by carrying out the phenol conversion over different metals (Pt, Pd, Rh, Ru, Ni and Co) supported on SiO₂. Silica was used as an inert support that enables to investigate only the effect of the metal.

2 Experimental

2.1 Catalyst Synthesis

SiO₂ (Aldrich) was calcined under air flow at 1073 K for 5 h. SiO₂ supported metal (Pt, Pd, Rh, Ru, Ni, Co) catalysts were prepared by incipient wetness impregnation of the support with aqueous solution of the respective precursor salts [Pt(NH₃)₄(NO₃)₂ (Aldrich), Pd(NO₃)₂·2H₂O (Umicore), RhCl₃·H₂O (Aldrich), Ru(NO)(NO₃)₃ (Alfa Aesar), Ni(NO₃)₂·6H₂O (Acros) and Co (NO₃)₂·6H₂O (Acros)]. After impregnation, the powder was dried in air at 293 K for 12 h and then calcined in air at 673 K for 3 h (2 K/min).

2.2 Catalyst Characterization

The chemical composition of each sample was determined on a Wavelength Dispersive X-Ray Fluorescence Spectrometer (WD-XRF) S8 Tiger (Bruker) with a rhodium tube operated at 4 kW. The analyses were performed with the samples (300 mg) in powder form using a semi-quantitative method (QUANT-EXPRES/Bruker). Specific surface areas of the samples were measured on a Micromeritics ASAP 2020 analyzer by N₂ adsorption at the boiling temperature of liquid nitrogen. The X-ray powder diffraction pattern of the calcined and reduced/passivated samples were obtained with CuKα radiation ($\lambda = 15,406 \text{ \AA}$) using a RIGAKU diffractometer. Data were collected over the 2θ range of 10° to 90° using a scan rate of 0.02°/step and a scan time of 1 s/step. TPR experiments were performed in a TPR/TPD 2900 Micromeritics system equipped with a thermal conductivity detector (TCD). The catalyst was pretreated at 673 K for 1 h under a flow of air prior to the TPR experiment in order to remove adsorbed species from the catalyst surface. The reducing mixture (10.0 % H₂/N₂) was passed through the sample (80–500 mg) at a flow rate of 30 mL/min and the temperature was increased to 1273 K at a heating rate of 10 K/min. The metal dispersion of Pd, Pt, and Rh was measured by CO chemisorption, using the dynamic adsorption method. Before adsorption, the samples (50 mg) were reduced under pure H₂ (60 ml/min) at 773 K for 1 h (10 K/min), cooled to room temperature, and flushed in He for 30 min. Then, 1 mL-pulses of 5 % CO in He were injected, until saturation was reached, as monitored on a quadrupole mass spectrometer (MKS Cirrus 200). For Ru, Ni and Co based catalysts, the metal dispersion was obtained from the diffractogram of reduced samples using the Scherrer equation. The calcined samples were reduced under pure hydrogen (30 mL/min) at 773 K for 1 h, purged under N₂ at the same temperature for 30 min and cooled to 298 K. The reactor was maintained at 209 K, using a mixture of

isopropyl alcohol and liquid nitrogen. Then, the catalyst was passivated with a 5 % O₂/He mixture for 1 h at 209 K.

2.3 Catalytic Activity

The vapor-phase conversion of the phenol was carried out in a fixed-bed quartz reactor, operating at atmospheric pressure of H₂ and 573 K. Prior to reaction, the catalyst was reduced in situ under pure hydrogen (60 mL/min) at 773 K for 1 h. The catalysts were diluted with inert material (SiC mass/catalyst mass = 3.0) to avoid hot-spot formation. The reactant mixture was obtained by flowing H₂ through the saturator containing phenol, which was kept at the specific temperature required to obtain the desired H₂/phenol molar ratio (about 60). To avoid condensation, all lines were heated at (523 K). The reaction products were analyzed by GCMS Agilent Technologies 7890A, using HP-Innowax capillary column and a flame-ionization detector (FID). Catalysts were evaluated at different W/F by varying the catalyst amount in the range of 2.5–160 mg. The W/F is defined as the ratio of catalyst mass (g) to organic feed mass flow rate (g/h). The product yield and selectivity for each product were calculated as follows:

$$\text{Yield (\%)} = \frac{\text{mol of product produced}}{\text{mol of phenol fed}} \times 100 \quad (1)$$

$$\text{Selectivity (\%)} = \frac{\text{mol of product produced}}{\text{mol of phenol consumed}} \times 100 \quad (2)$$

The turnover frequency was calculated by using the reaction rate for the formation deoxygenated products and the metal dispersion measured by CO chemisorption and XRD.

3 Results and Discussion

3.1 Catalyst Characterization

The metal loading, the surface area and the metallic dispersion of the samples are reported in Table 1. The surface area of Pt and Rh supported catalysts was similar to that one of silica (171 m²/g). For Pd, Ru, Ni and Co catalysts, the surface area slightly decreased after addition of metal. The metallic dispersion varied from 9 to 44 %.

X-ray diffraction patterns for all catalysts are shown in Fig. 1. All samples exhibited a broad diffraction peak corresponding to amorphous silica. For Pt/SiO₂ and Rh/SiO₂, only the line characteristic of silica is observed, whereas the diffractograms of Pd, Ru, Ni and Co based catalysts showed the lines of the respective oxides (PdO, NiO, Co₃O₄ and RuO₂). The absence of metal peaks in

Table 1 Metal composition, surface area, metal dispersion and turnover frequency for HDO of phenol

Catalysts	wt% Me	BET (m ² /g)	Dispersion (%) ^a	TOF _{HDO} ($\times 10^{-3}$ s ⁻¹)
Pt/SiO ₂	0.95	166	44	15.7
Pd/SiO ₂	0.55	155	15	7.2
Rh/SiO ₂	1.0	167	28	22.6
Ru/SiO ₂	3.8	143	15	24.1
Ni/SiO ₂	9.6	143	9	6.1
Co/SiO ₂	9.7	143	9	6.9

^a For Ru, Co and Ni catalysts, the dispersion was obtained using the diffractograms of reduced samples and the Scherrer equation. Metallic dispersion was calculated by CO chemisorption for Pt, Pd and Rh supported catalysts

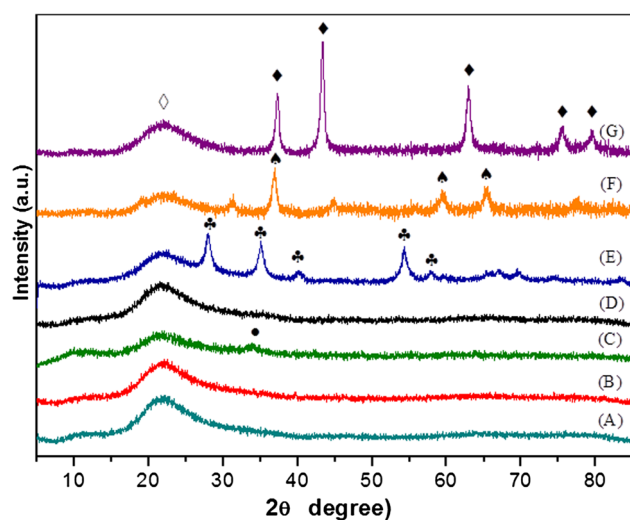


Fig. 1 XRD patterns of *a* SiO₂; *b* Pt/SiO₂; *c* Pd/SiO₂; *d* Rh/SiO₂; *e* Ru/SiO₂; *f* Co/SiO₂ and *g* Ni/SiO₂. (diamond) SiO₂; (filled circle) PdO; (filled diamond) NiO; (spade symbol) Co₃O₄; (claver symbol) RuO₂

XRD patterns of Pt/SiO₂ and Rh/SiO₂ is likely due to the high metallic dispersion rather than low metal loading since Pd/SiO₂ catalyst has the lowest metal loading (Table 1), but still shows a peak associated with PdO in XRD pattern.

The TPR profiles of all samples are shown in Fig. 2. Pt/SiO₂, Pd/SiO₂, Rh/SiO₂, Ru/SiO₂, and Ni/SiO₂ catalysts showed only one peak at 409, 332, 457, 521, and 737 K that corresponds to the reduction of the respective oxides (PtO₂, PdO, Rh₂O₃, RuO₂, and NiO). The broad hydrogen consumption at high temperature observed for Pd/SiO₂ catalysts could be attributed to the reduction of small PdO particles. For Co/SiO₂ catalyst, two peaks are observed, which are due to the two step reduction of cobalt oxide (Co₃O₄ → CoO → Co) [34]. All samples were completely reduced up to 773 K except for Co/SiO₂ catalyst that still exhibited hydrogen consumption up to 883 K.

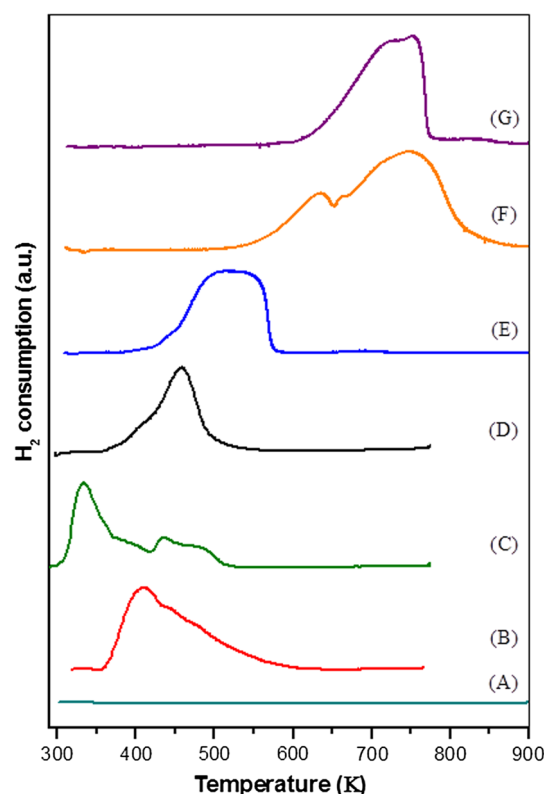


Fig. 2 TPR profiles of *a* SiO₂; *b* Pt/SiO₂; *c* Pd/SiO₂; *d* Rh/SiO₂; *e* Ru/SiO₂; *f* Co/SiO₂; *g* Ni/SiO₂

3.2 HDO of Phenol over Me/SiO₂ Catalysts

Figure 3 shows the phenol conversion and product yield at 573 K over Pt/SiO₂, Ru/SiO₂, and Ni/SiO₂ as a function of W/F. Silica support did not exhibited any activity even at the highest W/F used. Ni/SiO₂ catalyst showed the highest activity. For Pt/SiO₂ and Ni/SiO₂ catalysts, cyclohexanone and cyclohexanol were the main products formed along the entire W/F range, with small amounts of benzene and methane (Ni catalyst). By contrast, methane was the dominant product over Ru/SiO₂ catalyst, with only small

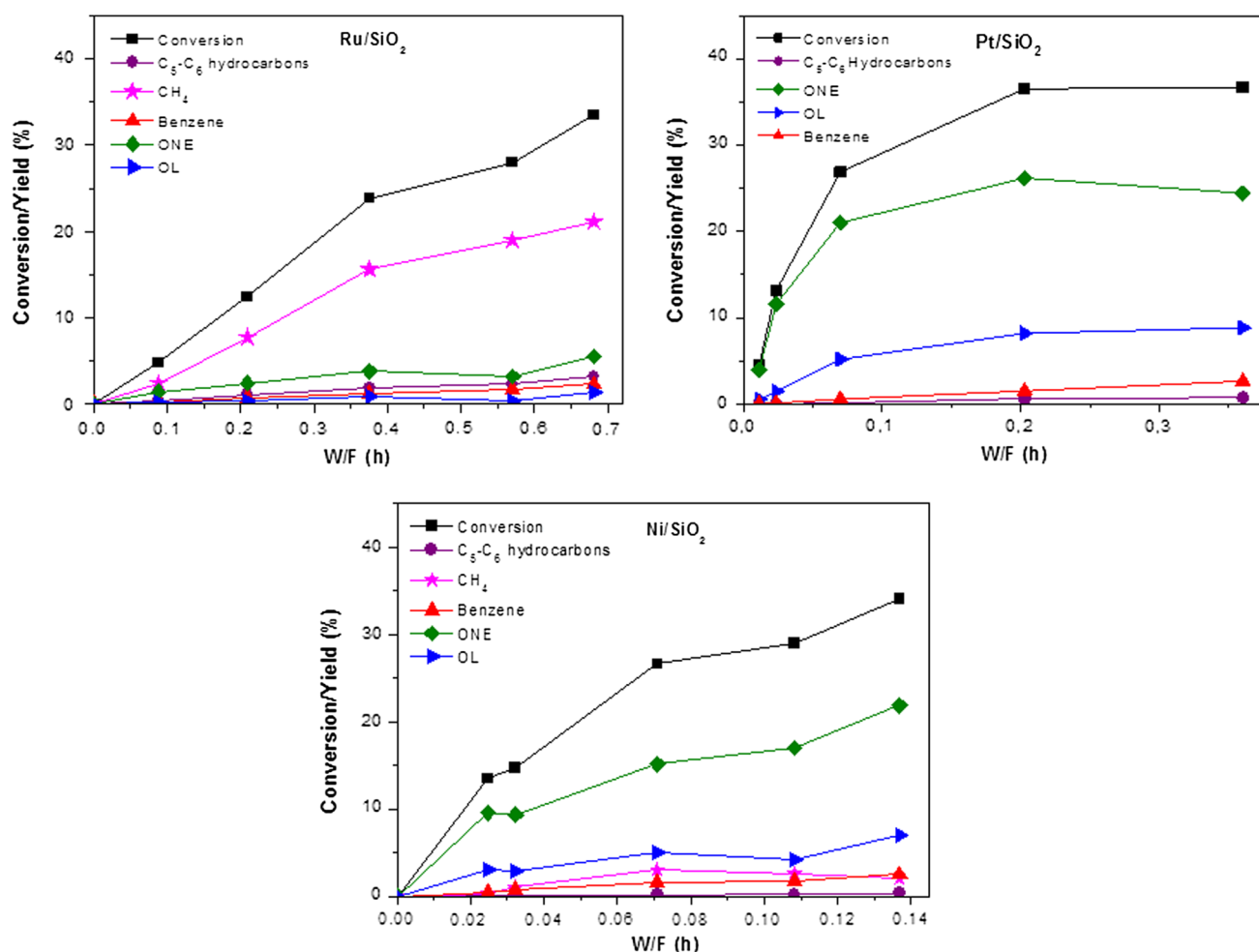


Fig. 3 Phenol conversion and yield of products for HDO of phenol as a function of W/F over Pt/SiO₂, Ru/SiO₂ and Ni/SiO₂ catalysts. Reaction conditions: T = 573 K, P = 1 atm, and H₂/phenol molar ratio 60. ONE—cyclohexanone, OL—cyclohexanol

amounts of cyclohexanone, benzene and C₅–C₆ hydrocarbons in the whole W/F range.

The TOF for HDO was calculated taking into account the data obtained under differential reaction conditions (conversion around 10 %) and the results are reported in Table 1. The TOF varied significantly with the type of metal. Rh/SiO₂ catalyst was 3 fold more active than Pd, Ni and Co-based catalysts. The following order of TOF was observed: Pd/SiO₂ ≈ Ni/SiO₂ ≈ Co/SiO₂ < Pt/SiO₂ < Rh/SiO₂ ≈ Ru/SiO₂. This result suggests that the type of metal strongly affects the deoxygenation activity.

The product distribution for HDO of phenol at 573 K over all silica supported catalysts at similar levels of conversion (around 10 %) is listed in Table 2. Cyclohexanone and cyclohexanol were basically the only products formed over Pt/SiO₂ and Pd/SiO₂ catalysts with small amounts of benzene. For Rh/SiO₂, Co/SiO₂ and Ni/SiO₂ catalysts, the selectivities to cyclohexanone and cyclohexanol are still

high but now, the formation of small amounts of benzene, C₅–C₆ hydrocarbons (*n*-hexane, 2-methyl-butane, cyclohexene, cyclohexane) and methane is also observed. In the case of Co/SiO₂ catalyst, the selectivities to cyclohexanone and cyclohexanol significantly decreased whereas a significant formation o-cresol (17.0 %) and small amounts of C₁₂ hydrocarbons is observed. The formation of C₁₂ hydrocarbons such as biphenyl, cyclohexylbenzene, 2-cyclohexylphenol and 2-phenylphenol have been reported for HDO of phenol over supported Pd catalysts [12]. Bicyclic hydrocarbons were formed probably from the alkylation of phenolic and aromatic rings by cyclohexanol or cyclohexanone over Lewis acid sites [35]. The hydrogenolysis of these C₁₂ compounds over Lewis acid sites is likely responsible for the formation of o-cresol [36]. In our work, SiO₂ does not exhibit any measurable acidity. Therefore, the Lewis acidity of Co/SiO₂ catalyst was likely created by the presence of unreduced Co species after reduction at

Table 2 Product distribution for HDO of phenol at 573 K and atmospheric pressure over silica supported metal catalysts

	Pt/SiO ₂	Pd/SiO ₂	Rh/SiO ₂	Ru/SiO ₂	Ni/SiO ₂	Co/SiO ₂
W/F (h)	0.023	0.151	0.045	0.209	0.032	0.089
Conversion (%)	13.2	17.1	9.4	12.4	14.7	11.3
Selectivity (%)						
ONE	88.0	93.7	85.3	19.4	63.6	35.9 (53.4) ^a
OL	11.0	3.0	4.2	3.4	20.0	12.0 (19.2)
Benzene	0.8	3.3	3.1	5.8	4.8	11.7 (10.0)
C ₅ –C ₆ hydrocarbons	–	–	7.2	8.7	1.2	5.0 (4.9)
CH ₄	–	–	–	62.3	7.2	13.6 (5.4)
C ₁₂ hydrocarbons	0.2	–	0.2	0.4	1.2	4.8 (1.2)
o-cresol	–	–	–	–	2.0	17.0 (5.9)

C₅–C₆ hydrocarbons—cyclohexane; cyclohexene; 2-methyl-butane; *n*-hexane. C₁₂ hydrocarbons—biphenyl; cyclohexylbenzene; pentylbenzene; 2-phenylphenol

^a Selectivities for HDO of phenol over Co/SiO₂ catalyst reduced at 873 K

773 K, as determined by TPR. In order to demonstrate the role of the unreduced Co species on the reaction mechanism, the HDO of phenol reaction was carried out over the Co/SiO₂ catalyst reduced at 873 K. According to TPR profile, the cobalt oxide is completely reduced at this temperature. In this case, the selectivity to bicyclic hydrocarbons and o-cresol significantly decreased whereas the formation of cyclohexanone increased, which agrees very well with the proposed reaction pathway. Ru/SiO₂ catalyst exhibits a high selectivity to methane (62.3 %) and C₅–C₆ hydrocarbons (8.7 %).

Pt/SiO₂ and Pd/SiO₂ catalysts were also tested for HDO of phenol at 623 K (Table 3). Increasing the reaction temperature significantly increased the formation of benzene and decreased the selectivity to cyclohexanone and cyclohexanol.

3.3 Proposed Reaction Pathway for Hydrodeoxygenation of Phenol

The reaction mechanism for HDO of phenol has been extensively studied in the literature. Recently, we investigated the performance of Pd catalysts supported on SiO₂, Al₂O₃ and ZrO₂ for the HDO of phenol in gas phase, at 573 K and 1 atm [12]. Pd supported on SiO₂ and Al₂O₃ exhibited high selectivity to cyclohexanone, whereas Pd supported on an oxophilic support such as ZrO₂ favored the selectivity towards benzene, reducing the formation of

ring-hydrogenated products, cyclohexanone and cyclohexanol. Diffuse reflectance infrared Fourier transform spectroscopy experiments revealed the participation of a keto-tautomer intermediate (2,4-cyclohexadienone) in the reaction. This intermediate can be hydrogenated in two different pathways. For Pd/SiO₂ and Pd/Al₂O₃ catalysts, the ring is hydrogenated and cyclohexanone and cyclohexanol are the main products formed. On the other hand, the hydrogenation of the carbonyl group of the keto-intermediate tautomer leads to the formation of benzene via rapid dehydration of the unstable cyclohexadienol intermediate. This is observed in the case of Pd/ZrO₂ catalyst. These results demonstrated that the selectivity for HDO of phenol can be controlled by using supports of varying oxophilicity.

In the present work, the results obtained revealed that the type of the metal also significantly affected product distribution for HDO of phenol. Comparing the product selectivities obtained for HDO of phenol at 573 K over silica supported catalysts, it is noticed the presence of two different groups of catalysts. For Pt, Pd and Rh based catalysts, the hydrogenation products (ONE and OL) were mainly formed. In order to enhance the deoxygenation activity of Pd and Pt-based catalysts, the HDO of phenol was carried out at 623 K. Increasing the reaction temperature significantly increased the formation of benzene and decreased the selectivity to cyclohexanone and cyclohexanol (Table 3). According to our previous work on Pd/SiO₂ catalyst, phenol is tautomerized to 2,4-cyclohexadienone

Table 3 Products distribution for HDO of phenol at 623 K and atmospheric pressure

Catalysts	Conversion (%)	Selectivity (%)				
		Benzene	ONE	OOL	ANE-ENE	C ₅ –C ₆
Pt/SiO ₂	9.2	24.8	61.6	8.0	1.8	3.4
Pd/SiO ₂	4.8	44.6	52.7	2.7	–	0.0

intermediate [12], followed by the hydrogenation of the ring, producing cyclohexanone and then cyclohexanol. For these catalysts, the sequential hydrogenation of the aromatic ring on metal sites followed by dehydration of cyclohexanol to benzene on acid sites cannot occur because silica does not exhibit sufficient acidity to catalyze the dehydration of cyclohexanol.

On the other hand, the more oxophilic metals such as Ru, Co and Ni promoted the formation of C–C bond hydrogenolysis products such as methane and C₅–C₆ hydrocarbons. The formation of hydrogenolysis products for HDO of phenolic compounds has been scarcely reported in the literature [21, 38], which is likely due to the fact that the majority of the works were performed in liquid phase.

Chen et al. [37] studied the HDO of *m*-cresol in gas phase at different temperatures over Pt/SiO₂, Pd/SiO₂ and Ni/SiO₂ catalysts. At 573 K, toluene and 3-methylcyclohexanone were the only products formed over Pt- and Pd-based catalysts whereas a significant formation of methane and phenol was also observed for Ni/SiO₂ catalyst. They proposed that the direct deoxygenation to toluene and the hydrogenation to methylcyclohexanone or methylcyclohexanol are the main reactions over all catalysts but products distribution varies depending on the metal. According to them, the oxygen removal occurs through an apparent direct hydrodeoxygenation that might involve the direct hydrogenolysis of the C–O bond or the tautomerization route. They ruled out the hydrogenation/deoxygenation route since the support has not enough acidity to catalyze dehydration of 3-methylcyclohexanol. For Ni-based catalyst, the hydrogenolysis of the C–C bond of the methyl group of the *m*-cresol molecule produces methane and phenol. However, they did not explain the reasons for the higher hydrogenolysis activity on Ni/SiO₂ catalyst.

A comprehensive study was performed about the HDO of *m*-cresol in gas phase at 573 K over different silica supported catalysts (Pd, Pt, Ru, Ni, Fe, NiFe) [10, 11, 21]. Hydrogenation products (3-methylcyclohexanone and 3-methylcyclohexanol) were the main products formed over Pt/SiO₂, Pd/SiO₂ and Ni/SiO₂ catalysts whereas toluene was the dominant product on Fe and Ni–Fe bimetallic catalysts. Ru/SiO₂ catalyst showed significant formation of toluene as well as CH₄ and C₂–C₆ hydrocarbons. The differences in product distributions were explained in terms of a complex reaction pathway that depended on the type of metal. For Pt/SiO₂, Pd/SiO₂, Ni/SiO₂, Fe/SiO₂, NiFe/SiO₂ catalysts, the reaction mechanism involves the formation of a keto-tautomer intermediate (3-methyl-3,5-cyclohexadienone). This tautomer can undergo the hydrogenation of the ring, producing 3-methylcyclohexanone, or the hydrogenation of the carbonyl group, leading the formation of 3-methyl-3,5-

cyclohexadienol. The reaction pathway depends on the nature of metallic phase. The presence of an oxophilic metal, such as the partially reduced Fe species present in the NiFe/SiO₂ catalysts promoted the hydrogenation of the carbonyl group of the tautomer intermediate. On the other hand, instead of the tautomerization route, the direct dehydroxylation of *m*-cresol is favored over Ru based catalyst. In this case, DFT calculations showed a higher reaction energy and energy barrier for the hydrogenation of the O in the carbonyl group of the keto tautomer due to a stronger interaction of the O with Ru than with Pt. It was proposed that the direct dehydroxylation produces a partially unsaturated hydrocarbon species, which may be hydrogenated to toluene or may undergo C–C bond breaking, producing C₁–C₅ hydrocarbons. Therefore, the oxophilicity of the metal surface can determine the reaction pathway. For oxophilic metals such as Ru and Fe, the deoxygenation is promoted whereas the hydrogenation is favored over less oxophilic metals such as Pt, Pd or Ni. In addition, this reaction mechanism may also explain the formation of hydrogenolysis products for HDO of phenolic compounds on some catalysts.

According to this mechanism, the stabilization of the tautomer intermediate on the surface of these metals is fundamental in determining the reaction pathway. A higher stabilization of the tautomer intermediate on the metal particle increases the energy barrier for the hydrogenation of the carbonyl group, favoring the direct deoxygenation. Therefore, the deoxygenation activity depends on the affinity of the metals to bond with oxygen from carbonyl group, as it was also proposed by Mortensen et al. [6].

Mortensen et al. [6] studied the HDO of phenol in liquid phase over Ru/C, Pd/C and Pt/C. Cyclohexane was the main product formed over Ru/C catalyst whereas Pd/C and Pt/C produced mainly cyclohexanol. They reported the following order of activity for deoxygenation for HDO of phenol: Ru/C > Pd/C > Pt/C. Based on the work of Norskov et al. [38], the authors proposed a correlation between the affinity of the metals to bind oxygen and their deoxygenation activity. Therefore, the best performance to deoxygenation of Ru-based catalyst was due to its strongest binding energy with respect to oxygen than Pt or Pd.

In order to investigate the relationship between the deoxygenation activity and the affinity of the metals to bond with oxygen from carbonyl group, we took into account the work of Lee et al. [39]. They studied the hydrogenation of acetaldehyde to ethanol in liquid phase over different metals (Pd, Pt, Rh, Ru, Ni, Co). Acetaldehyde may be bonded to the metal surface either through the oxygen atom ($\eta^1(\text{O})$ configuration) or via the oxygen and carbon atoms of the carbonyl group ($\eta^2(\text{C},\text{O})$ configuration) [40]. The adsorption configuration depends on the

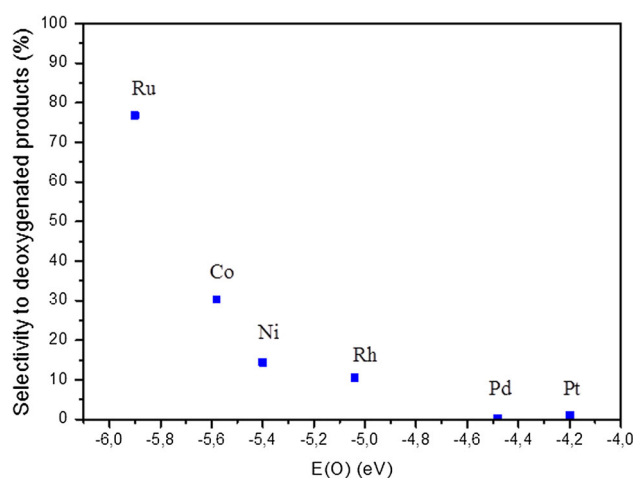


Fig. 4 Selectivity to deoxygenated products as a function of the binding energies of atomic oxygen calculated by Lee et al. [39]

type of the metal. Therefore, they used DFT to calculate the binding energies of atomic C and O on the different metal surfaces. Oxygen binds more strongly to Ru than the other metals. The following binding energies of atomic oxygen were observed: Ru (-5.90) < Co (-5.58) < Ni (-5.40) < Rh (-5.04) < Pd (-4.48) < Pt (-4.20).

The selectivity to deoxygenated products obtained in our work was plotted as a function of the binding energies of

atomic oxygen calculated by Lee et al. [39] and the results are shown in Fig. 4. The selectivity to deoxygenated products increased in the same order of binding energies of atomic oxygen. These results clearly demonstrated that stronger bind of oxygen from carbonyl group to metal, favors the formation of deoxygenated products.

A similar relationship could be obtained by plotting the selectivity to deoxygenated products for HDO of phenol and the Me–O bond dissociation energies [41]. There is a reasonable correlation, taking into account the estimated errors (Fig. S1). In addition, the trend was similar to that one obtained considering the data from Lee et al. [39]. However, the relationship between the binding energy of oxygen from the carbonyl group and the selectivity to deoxygenated products seems to represent more effectively our proposal, which is based on the adsorption of oxygen atom from the carbonyl group of the tautomer formed (2,4-cyclohexadienone). This is likely the reason for the best fitting of the selectivity to deoxygenated products of our work with the data reported by Lee et al. [39].

Therefore, a complete HDO of phenol reaction pathways over silica supported metal catalysts is proposed in Scheme 1, representing the main reaction route for each metal.

Besides the effect of the type of the metal, it could be argued that the changes in product distribution are due to the different metal dispersion of the catalysts studied in this

Scheme 1 Reaction pathways for HDO of phenol over silica supported metal catalysts

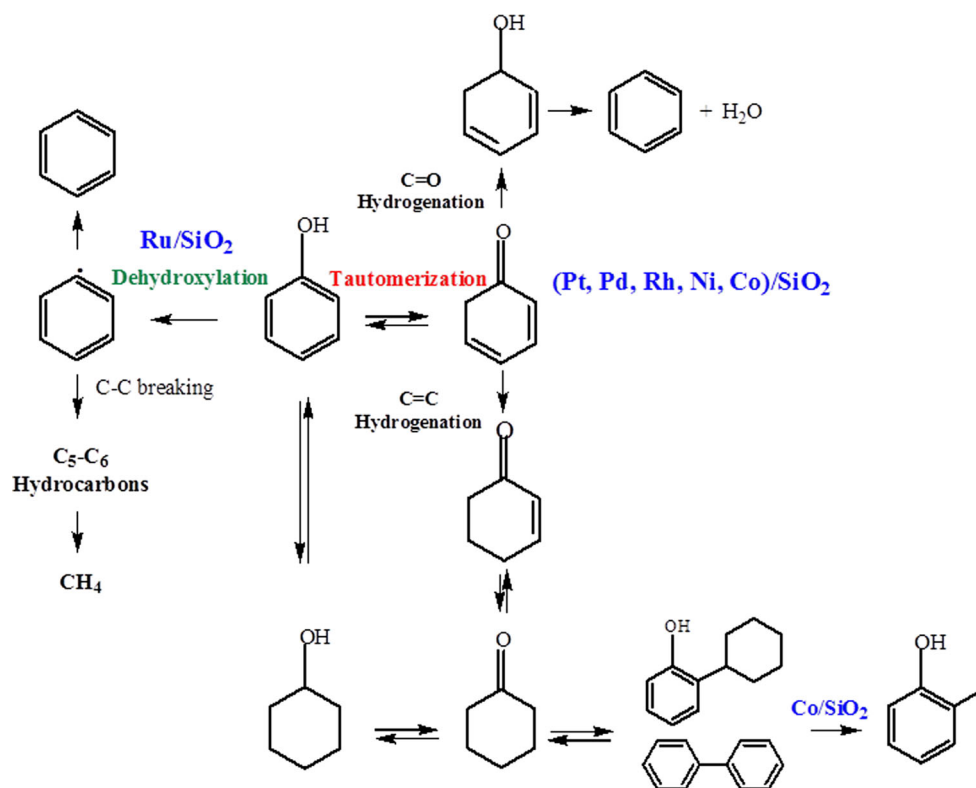


Table 4 Products distribution for HDO of phenol at 573 K and atmospheric pressure

Catalysts	Dispersion (%)	Conversion (%)	Selectivity (%)				
			Benzene	ONE	OL	CH ₄	C ₅ –C ₆
Ni/SiO ₂	5.4	10.1	4.9	69.6	23.8	1.2	0.3
Ni/SiO ₂	9.0	12.0	3.1	71.3	23.0	2.0	–
Ru/SiO ₂	6.0	5.0	5.4	30.4	6.7	45.7	12.0
Ru/SiO ₂	15.0	4.8	6.0	30.5	4.0	50.2	9.0

work. However, the effect of the metal dispersion for HDO of phenol reaction is controversial in the literature [12, 25, 42]. Newman et al. [25] and Mortensen et al. [42] reported an influence of metal particle size on the HDO of phenol in liquid phase over Ru and Ni supported catalysts, respectively. However, the effect of Pd particle size on the product distribution for HDO of phenol in gas phase over Pd/ZrO₂ catalysts with different Pd dispersions was previously investigated [12]. Both catalysts exhibited similar selectivities indicating that metal dispersion does not significantly affect the product distribution in the HDO of phenol.

Therefore, the HDO of phenol in gas phase at 573 K was carried out over Ni/SiO₂ and Ru/SiO₂ catalysts with different metal dispersion in order to investigate the effect of metal particle size on product distribution. The selectivity obtained at low phenol conversion is listed in Table 4. For Ni/SiO₂ catalyst, decreasing Ni dispersion from 9 to 5 % did not change the selectivity to all products. When Co/SiO₂ is compared with the Ni/SiO₂ catalyst with the same dispersion (9 %), it is clear that the differences in product distribution are due to the type of the metal. Ru/SiO₂ catalyst exhibited a product distribution quite different from the other catalysts. In particular, it was noticed a significant formation of hydrogenolysis products such as methane and C₅–C₆ hydrocarbons. However, the selectivity to hydrogenolysis products was approximately the same for both Ru/SiO₂ catalysts with different metal dispersion. In addition, Ru/SiO₂ and Pd/SiO₂ catalysts have the same metal dispersion but the selectivities are quite different, which demonstrated the key role of the type of the metal on catalyst performance.

4 Conclusions

The effect of metal type for the HDO of phenol in gas phase was investigated over silica supported catalysts. Pt/SiO₂, Pd/SiO₂ and Rh/SiO₂ catalysts favor the formation of hydrogenated products (cyclohexanone and cyclohexanol), whereas Co/SiO₂, Ni/SiO₂ and mainly Ru/SiO₂ catalysts exhibits significant formation of hydrogenolysis products (C₅–C₆ hydrocarbons and methane). Two different reaction pathways take place depending on the type of the metal.

For Pt/SiO₂, Pd/SiO₂ and Rh/SiO₂ catalysts, phenol is mainly tautomerized, followed by hydrogenation of the C–C bond of the tautomer intermediate formed, producing cyclohexanone and cyclohexanol. By contrast, the direct dehydroxylation of phenol followed by hydrogenolysis might also occur over more oxophilic metals such as Ru, Co and Ni. This is supported by a correlation between deoxygenation activity and metals affinity to bond with oxygen.

Acknowledgments Camila A. Teles and Jerusa R. de Lima thank CAPES (Coordenação de Aperfeiçoamento de Pessoal de Ensino Superior) for the scholarship received.

References

- Wang Y, Wu J, Wang S (2013) RSC Adv 3:12635–12640
- Huber GW, Iborra S, Corma A (2006) Chem Rev 106:4044–4098
- Mortensen PM, Grunwaldt JD, Jensen PA, Knudsen KG, Jensen AD (2011) Appl Catal A 407:1–19
- Zanuttini MS, Dalla Costa BO, Querini CA, Peralta MA (2014) Appl Catal A 482:352–361
- Massoth FE, Politzer P, Concha MC, Murray JS, Jakowski J, Simons J (2006) J Phys Chem B 110:14283–14291
- Mortensen PM, Grunwaldt JD, Jensen PA, Jensen AD (2013) ACS Catal 3:1774–1785
- Liu H, Jiang T, Han B, Liang S, Zhou Y (2009) Science 326:1250–1252
- Velu S, Kapoor MP, Inagaki S, Suzuki K (2003) Appl Catal A 245:317–331
- Hong DY, Miller SJ, Agrawal PK, Jones CW (2010) Chem Commun 46:1038–1040
- Nie L, De Souza PM, Noronha FB, An W, Sooknoi T, Resasco DE (2013) J Mol Catal A 388:47–55
- De Souza PM, Nie L, Borges LEP, Noronha FB, Resasco DE (2014) Catal Lett 144:2005–2011
- De Souza PM, Rabelo-Neto RC, Borges LEP, Jacobs J, Davis BH, Sooknoi T, Resasco DE, Noronha FB (2015) ACS Catal 5:1318–1329
- De Souza PM, Rabelo-Neto RC, Borges LEP, Jacobs G, Davis BH, Graham UM, Resasco DE, Noronha FB (2015) ACS Catal 5:7385–7398
- Senol OI, Ryymin EM, Viljava TR, Krause AOI (2007) J Mol Catal A 277:107–112
- Sun Q, Chen G, Wang H, Liu X, Han J, Ge Q, Zhu X (2016) ChemCatChem 8:551–561
- Foster AJ, Do PTM, Lobo RF (2012) Top Catal 55:118–128
- Hensley AJR, Wang Y, McEwen JS (2015) ACS Catal 5:523–536
- Zhao C, Kasakov S, He J, Lercher JA (2012) J Catal 296:12–23
- Furimsky E (2000) Appl Catal A 199:147–190

20. Nie L, Resasco DE (2014) *J Catal* 317:22–29
21. Tan Q, Wang G, Nie L, Dinse A, Buda C, Shabaker J, Resasco DE (2015) *ACS Catal* 11:6271–6283
22. Echeandia S, Pawelec B, Barrio VL, Arias PL, Cambra JF, Loricera CV, Fierro JLG (2014) *Fuel* 117:1061–1073
23. Zhao C, He J, Lemonidou AA, Li X, Lercher J (2011) *J Catal* 280:8–16
24. Horacek J, St'ávoová G, Kelbichová V, Kubicka D (2013) *Catal Today* 204:38–45
25. Newman C, Zhou X, Goundie B, Ghampson IT, Pollock RA, Ross Z, Wheeler MC, Meulenberg R, Austin RN, Frederick BG (2014) *Appl Catal A* 477:64–74
26. Do PTM, Foster AJ, Chen J, Lobo RF (2012) *Green Chem* 14:1388–1398
27. Wan H, Chaudhari RV, Subramaniam B (2012) *Top Catal* 55:129–139
28. Zhu X, Nie L, Lobban LL, Mallinson RG, Resasco DE (2014) *Energy Fuels* 28:4104–4111
29. Hong Y, Zhang H, Sun J, Ayman KM, Hensely AJR, Gu M, Engelhard MH, McEwen J-S, Wang Y (2014) *ACS Catal* 4:3335–3345
30. Shin EJ, Keane MA (2000) *Ind Eng Chem Res* 39:883–892
31. Zhao C, Camaioni DM, Lercher JA (2012) *J Catal* 288:92–103
32. Zhang X, Wang T, Ma L, Zhang Q, Huang X, Yu Y (2013) *Appl Energy* 112:533–538
33. Guvenatam B, Kursun O, Heeres EHJ, Pidko EA, Hensen EJM (2013) *Catal Today* 233:83–91
34. Noronha FB, Perez CA, Schmal M, Frety R (1999) *Phys Chem Chem Phys* 1:2861–2867
35. Nimmanwudipong T, Runnebaum RC, Tay K, Block DE, Gates BC (2011) *Catal Lett* 141:1072–1078
36. Kallury RKMR, Tidwell TT, Boocock DGB, Chow DHL (1984) *Can J Chem* 62:2540–2545
37. Chen C, Chen G, Yang F, Wang H, Han J, Ge Q, Zhu X (2015) *Chem Eng Sci* 135:145–154
38. Norskov JK, Rossmeisl J, Logadottir A, Lindqvist L (2004) *J Phys Chem B* 108:17886–17892
39. Lee J, Xu Y, Huber GW (2013) *App. Catal. B: Environ.* 140:98–107
40. Ferrin P, Simonetti D, Kandoi S, Kunkes E, Dumesic JA, Norskov JK, Mavrikakis M (2009) *J Am Chem Soc* 131:5809–5815
41. Bond dissociation energies. <https://labs.chem.ucsb.edu/zakarian/armen/11—bonddissociationenergy.pdf>. Accessed 13 July 2016
42. Mortensen PM, Grunwaldt JD, Jensen PA, Jensen AD (2016) *Catal Today* 277:297